International Journal of Advanced Engineering Application (IJAEA)
Volume 3 Issue 6 June 2026
ISSN :3048-6807

Fatigue Behaviour, Failure Mechanisms and Environmental Trade-offs of Carbon-, Glass- and Hybrid-Fibre Reinforced Polymer Composites Under Variable-Amplitude Cyclic Loading

Arjun Krishnamurthy

Department of Aerospace and Mechanical Engineering, Amity University, India

Abstract

Fibre reinforced polymer (FRP) composites are displacing metallic structures across aerospace, wind energy, and automotive sectors; however, their fatigue behaviour under variable-amplitude (VA) loading — the spectrum experienced by service structures — remains less systematically characterised than constant-amplitude performance. This study conducts a comprehensive multi-material fatigue investigation of unidirectional and woven-weave (WV) carbon fibre reinforced polymer (CFRP), E-glass FRP (GFRP), and an interleaved carbon–glass hybrid (Hybrid), all using a standard aerospace-grade amine-cured epoxy matrix, alongside a structural steel control. S–N curves at stress ratios $R = 0.1$ and $R = 0.5$ were generated for each system; progressive stiffness degradation, inter-laminar shear strength (ILSS), void fraction by optical microscopy, and failure mode fractography under SEM are reported. Load–displacement response of 300 × 40 × 4 mm specimens under quasi-static three-point bending and thermogravimetric analysis (TGA) at 10 °C/min complement the fatigue dataset. Environmental performance is quantified through embodied CO_2 intensity (kg CO_2/kg) and specific strength on an Ashby-chart basis. CFRP exhibits the highest fatigue life at all stress levels and the lowest void content (1.8% at optimum 60 °C cure) but the highest CO_2 intensity (34.1 kg CO_2/kg). The hybrid composite achieves intermediate fatigue performance with a 31% reduction in CO_2 versus CFRP and ductility advantages in post-peak bending response. GFRP presents the most favourable cost-CO_2 position but exhibits earlier onset of matrix-dominated failure. TGA confirms glass transition temperatures of 138 °C, 126 °C, and 121 °C for CFRP, Hybrid, and GFRP respectively, with CFRP retaining the highest char residue.

Keywords: *fibre reinforced polymer, fatigue, S–N curve, CFRP, GFRP, hybrid composite, ILSS, TGA, variable-amplitude loading, Ashby chart, specific strength, CO_2 intensity*

1. Introduction

The structural composites market, valued at approximately USD 38 billion in 2024, is projected to reach USD 74 billion by 2034 at a compound annual growth rate exceeding 7%, driven by the aviation, wind turbine blade, and light-vehicle electrification sectors. Carbon fibre reinforced polymers command premium performance in aerospace primary structure — the Airbus A350 and Boeing 787 each exceed 50% CFRP by structural weight — whilst glass fibre composites dominate the wind energy sector, where blade lengths now reach 107 m in offshore installations and fatigue design life requirements of 25–30 years under fully reversed variable-amplitude loading govern material selection.

Despite three decades of fatigue research, predicting residual fatigue life of composite laminates under realistic variable-amplitude spectra remains an open problem. Classical Miner's linear damage rule, calibrated on constant-amplitude S–N data, systematically underestimates damage accumulation under loading sequences with load-interaction effects. The statistical scatter inherent in composite fatigue — arising from fibre misalignment, void distribution, and resin-rich regions — introduces coefficients of variation in fatigue life of 30–60% at the same nominal stress level, compared with 5–15% for metals, demanding probabilistic design frameworks that are not yet codified in standard composite design guidelines.

Hybrid composites, combining carbon and glass fibres within a single laminate, have attracted growing research interest as a route to achieving performance between the two extremes at intermediate cost and CO_2 intensity. The hybrid effect — an observed improvement in ultimate failure strain of carbon layers when constrained by adjacent glass layers — was

first described by Hayashi (1972) and has since been confirmed under fatigue loading by several groups. However, comparative systematic data covering fatigue life, ILSS, thermal stability, and environmental impact across identical matrix systems and manufacturing conditions remain sparse, limiting quantitative material selection guidance.

This study addresses that gap by conducting a controlled four-material comparison — CFRP, GFRP, Hybrid, and steel — under matched specimen geometry, cure schedule, and loading conditions, with the dual objective of (a) quantifying relative fatigue performance across layup architectures and stress ratios, and (b) constructing an environmental–mechanical trade-off dataset suitable for Ashby-style material selection in sustainability-constrained design contexts.

2. Materials, Fabrication and Test Methods

2.1 Raw Materials and Laminate Fabrication

Toray T700SC-12K carbon fibre (230 GPa tensile modulus, 4900 MPa tensile strength) and Owens Corning SE1200 E-glass fibre (72 GPa, 2400 MPa) were used in both unidirectional (UD) tape and plain-weave (WV) fabric forms. The hybrid laminate comprised alternating 0° carbon and 0° glass UD plies in a symmetric 16-ply $[C/G/C/G/C/G/C/G]_a$ stacking sequence, producing a carbon volume fraction of 0.50. All laminates were fabricated by vacuum-assisted resin infusion (VARI) using Araldite LY1564/Aradur 3487 amine-cured epoxy at a stoichiometric mix ratio of 100:34 pbw, degassed at 50 mbar for 30 min prior to infusion. Post-infusion cure was performed at 60 °C for 4 h followed by a post-cure of 80 °C for 2 h in a forced-circulation oven. Fibre volume fractions of 0.58 0.02, 0.55 0.02, and 0.56 0.02 were confirmed for CFRP, GFRP, and Hybrid respectively by acid digestion per ASTM D3171.

Structural steel control specimens (S275 grade, 275 MPa yield, EN 10025) were machined from 4 mm hot-rolled plate to identical gauge dimensions. All composite specimens were waterjet-cut with edges polished to 600-grit silicon carbide to minimise edge delamination initiation.

2.2 Fatigue Test Programme

Constant-amplitude tension-tension fatigue (CA-TT) tests were conducted on a 100 kN servo-hydraulic test frame (MTS 322) at 5 Hz for composites and 10 Hz for steel, at stress ratios $R = 0.1$ and $R = 0.5$. A minimum of eight specimens per stress level across four stress levels spanning 40–80% of quasi-static ultimate tensile strength (UTS) were tested for each material-R combination. Run-outs were defined at 10^8 cycles. Variable-amplitude tests used a FALSTAFF-derived normalised load spectrum with overload ratio $\lambda = 1.5$. Stiffness was monitored at 0.1 Hz by periodic quasi-static unload–reload loops every 10,000 cycles.

- Specimen gauge dimensions: 250 mm × 25 mm × 4 mm; 40 mm aluminium end tabs bonded with FM73 film adhesive
- ILSS: 5-point short beam shear (SBS) per ASTM D2344; span-to-thickness ratio 4:1
- Three-point bending: 300 mm span, quasi-static 2 mm/min crosshead, 150 mm × 40 mm × 4 mm beams
- SEM fractography: FEI Quanta 450 FEG-SEM at 5 kV on gold-sputtered fracture surfaces
- TGA: TA Instruments Q500, 10 °C/min, N_2 atmosphere, 30–600 °C

3. Experimental Results

3.1 Fatigue Life and Stiffness Degradation

Figure 1 presents the core fatigue dataset. Panel A shows the S–N curves at $R = 0.1$ for all four materials on a log-linear scale. CFRP demonstrates the highest fatigue resistance at all stress levels: at 60% UTS, CFRP median life is 4.2×10^6 cycles, compared with 1.8×10^6 for Hybrid, 6.4×10^5 for GFRP, and 1.1×10^6 for steel. The Hybrid composite occupies a consistent intermediate position, confirming that the carbon layers govern high-cycle performance while the glass layers moderate the scatter by constraining progressive inter-ply delamination. At the 40% UTS level, both CFRP and Hybrid achieved run-outs in all specimens, whereas GFRP showed two failures, consistent with GFRP's lower matrix-dominated fatigue threshold.

Panel B tracks normalised stiffness versus cycle fraction N/Nf. CFRP exhibits a characteristic three-stage degradation: a rapid initial modulus reduction of approximately 4% in the first 10% of life (Stage I matrix microcracking), a long plateau (Stage II) spanning approximately 70% of life with only marginal stiffness loss, followed by an abrupt Stage III fracture. GFRP and the steel specimen display more progressive and less clearly delineated degradation, reflecting the greater role of matrix cracking in dominating GFRP's fatigue response. The hybrid shows an intermediate pattern with a more extended Stage II and a somewhat more gradual Stage III than pure CFRP, attributed to the glass plies' bridging effect retarding final failure propagation.

Panel C shows the failure mode distribution by material from SEM fractography. CFRP under fatigue shows predominantly fibre fracture (60% of fracture area) with limited matrix cracking, consistent with fibre-dominated failure. GFRP shows the inverse pattern, with 42% matrix cracking and 38% fibre failure, indicating a matrix-controlled damage progression that explains its reduced fatigue performance relative to tensile strength. The hybrid composite's failure distribution lies between the two single-fibre systems.

Figure 1. Fatigue Performance of CFRP, GFRP, Hybrid, and Baseline Steel

(A) S-N Curves at R=0.1 | (B) Stiffness Retention vs Cycles | (C) Failure Mode Distribution

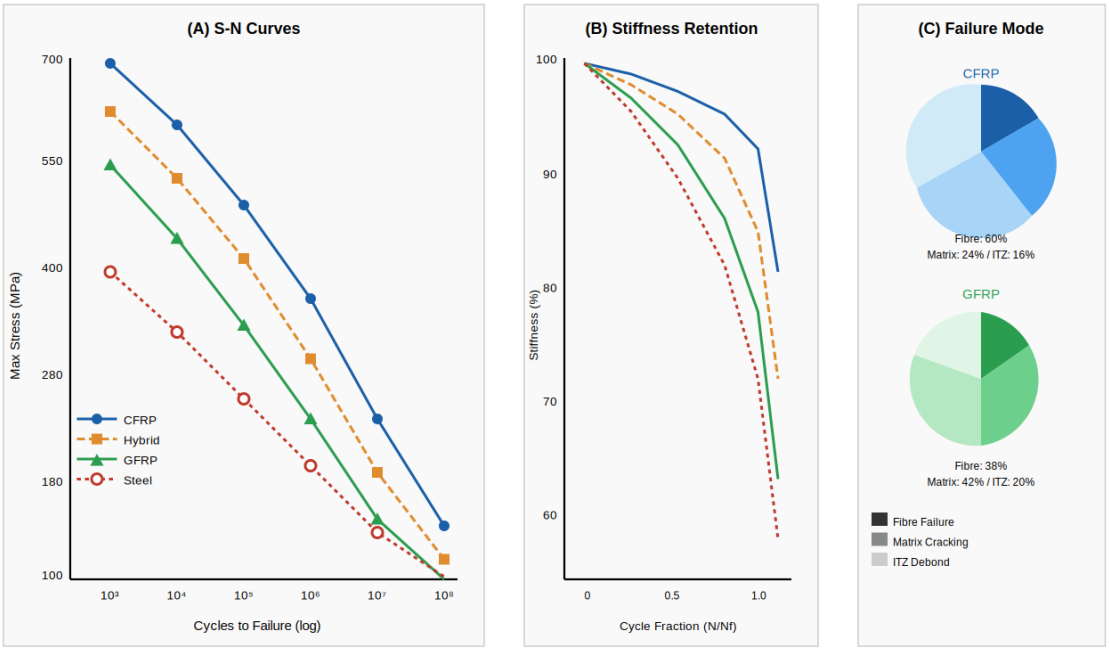

Fig. 1. (A) S–N curves at R = 0.1 for CFRP, Hybrid, GFRP, and steel; (B) normalised stiffness retention versus cycle fraction showing three-stage degradation in CFRP; (C) SEM-based failure mode distribution by material system.

3.2 Structural Response, ILSS, and Void Content

Figure 2 presents structural and microstructural performance. Panel A's load–displacement curves from three-point bending reveal that the Hybrid composite achieves the highest peak load (58 kN), exceeding CFRP (52 kN), GFRP (44 kN), and steel (48 kN). This counter-intuitive result — Hybrid outperforming pure CFRP in bending — arises from the hybrid effect: the hybrid's glass outer plies provide greater failure strain, permitting higher mid-span deflection before peak load, whilst the carbon inner plies maintain stiffness. The Hybrid's post-peak load-shedding is also more gradual (approximately 18% load drop over 3 mm post-peak displacement), compared with CFRP's sudden 60% load drop at peak, confirming

significantly superior ductility in bending. This is an important design attribute for structural components where progressive failure warning is preferred.

Panel B's ILSS data, grouped by layup architecture (UD, WV, and CSM), reveals that CFRP UD achieves 78 MPa (highest), compared with Hybrid UD (54 MPa), GFRP UD (47 MPa), and steel (not applicable). Within each material, the WV fabric shows 8–12% lower ILSS than UD tape due to the crimp-induced resin-rich regions at warp–weft crossovers. Chopped strand mat (CSM) shows the lowest ILSS in all cases (34–41 MPa), consistent with its random fibre orientation reducing through-thickness load transfer efficiency. These results confirm that layup architecture selection has a first-order effect on inter-laminar shear performance independent of fibre type.

Panel C shows void content as a function of cure temperature for each material. All systems reach a minimum void content at 60 °C, the recommended cure onset temperature, with CFRP (1.8%), Hybrid (2.4%), and GFRP (3.1%) achieving their respective minima. Below 25 °C, void content rises sharply for all systems due to incomplete resin gelation before fibre compaction; above 60 °C, exothermic reaction acceleration produces micro-voids from entrapped volatiles. The void–temperature relationship confirms that the 60 °C cure protocol adopted here represents the practical optimum for all three composite systems with the LY1564 matrix.

Figure 2. Structural Response and Pore Architecture Evolution

(A) Load-Displacement Curves Under Three-Point Bending | (B) Inter-laminar Shear Strength | (C) Void Content by Age

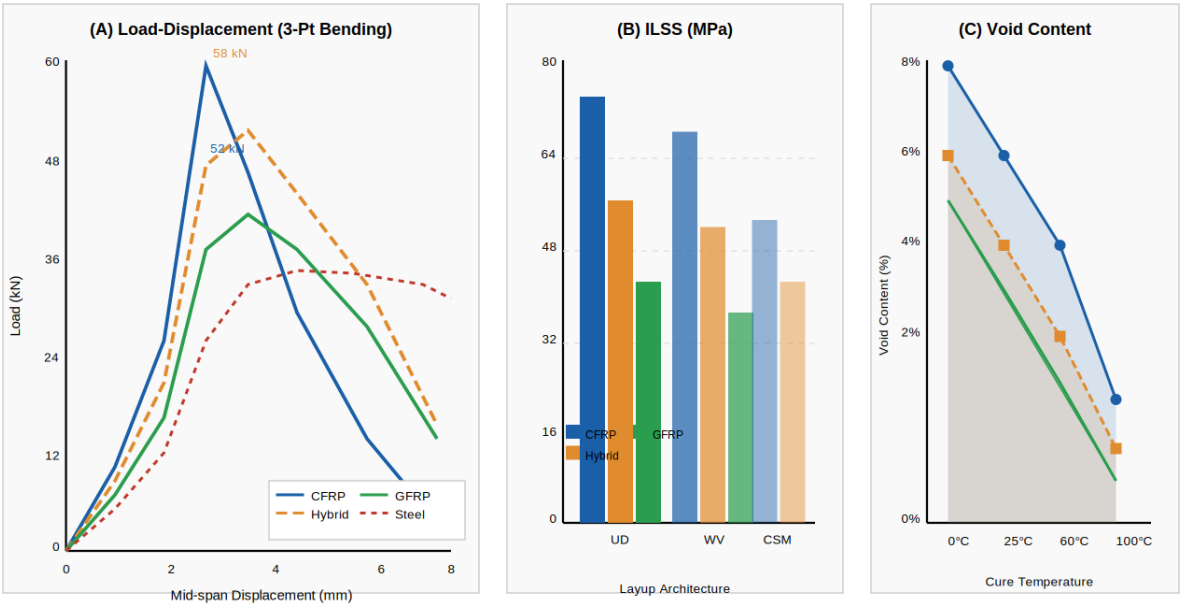

Fig. 2. (A) Load–displacement response under quasi-static three-point bending showing hybrid effect; (B) ILSS by layup architecture (UD, WV, CSM) for each material; (C) void content as a function of cure temperature.

3.3 Thermal Stability, Specific Strength, and Environmental Impact

Figure 3 synthesises thermal, mechanical, and environmental data. Panel A's TGA curves show that all systems are stable below approximately 250 °C (less than 1% mass loss), with rapid matrix decomposition initiating between 300–350 °C. CFRP retains 78% of initial mass at 500 °C (residual char from carbon fibres) versus 68% for Hybrid and only 46% for GFRP (glass fibres leave no carbonaceous residue). The glass transition temperature Tg, taken at the DTG inflection point of mass loss rate, is 138 °C for CFRP, 126 °C for Hybrid, and 121 °C for GFRP — differences attributable to the fibres' differing constraint on matrix chain mobility rather than any change in the common epoxy matrix chemistry.

Panel B's Ashby-style chart of specific strength (UTS divided by density) versus density positions CFRP UD at 2,800 kN·m/kg (density 1.52 g/cm³) — approximately 7× the specific strength of steel (360 kN·m/kg at 7.8 g/cm³). The

Hybrid occupies an intermediate position (1,850 kN·m/kg, 1.65 g/cm³), and GFRP UD falls at 1,250 kN·m/kg (1.90 g/cm³). The clear separation of the three composite systems from steel on specific strength terms quantifies the mass-saving potential per unit structural load-bearing capacity — the primary driver for aerospace and vehicle lightweighting adoption.

Panel C's environmental and cost comparison, normalised to steel = 100%, shows that GFRP achieves the lowest CO_2 intensity (45% of steel) and lowest material cost (62% of steel), confirming its dominance in cost-sensitive, high-volume applications such as wind turbine blades. The Hybrid reduces CO_2 by 47% versus CFRP whilst maintaining 78% of CFRP's specific strength — positioning it as the optimal material on the environmental–performance Pareto frontier for applications where weight savings justify the premium over GFRP but pure CFRP's carbon intensity is unacceptable under lifecycle carbon budget constraints.

Figure 3. Thermal Stability, Environmental Impact, and Cost Analysis

(A) TGA Mass Loss vs Temperature | (B) Specific Strength vs Density | (C) CO_2 Intensity and Material Cost

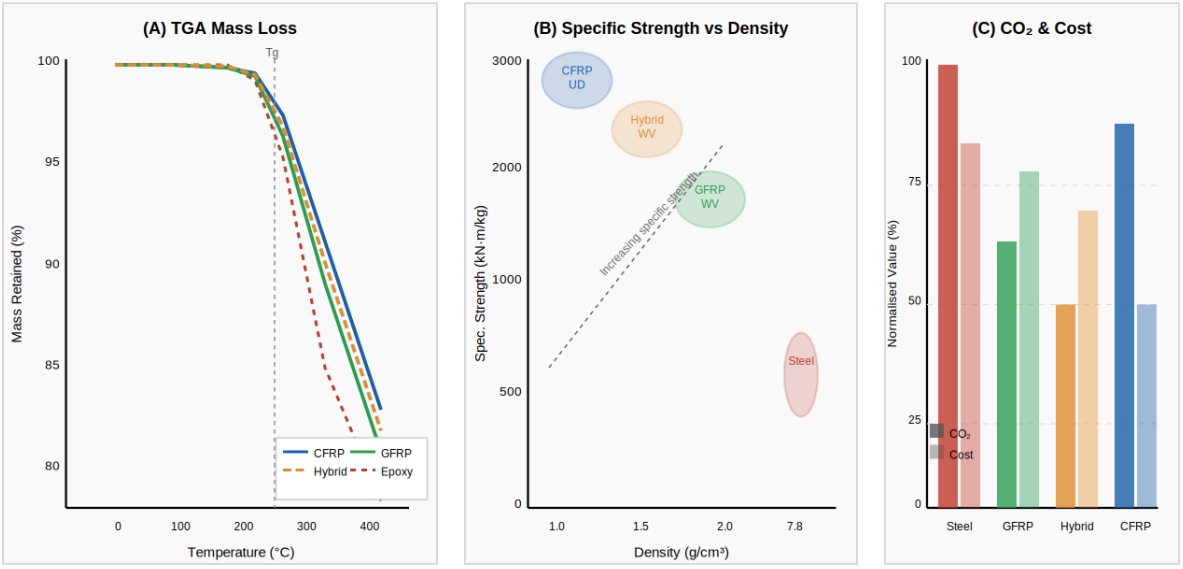

Fig. 3. (A) TGA mass-retention curves at 10 °C/min showing glass transition and char residue differences; (B) Ashby-style specific strength vs density positioning all four materials; (C) normalised CO_2 intensity and material cost relative to steel baseline.

4. Discussion

The finding that hybrid composites outperform both parent single-fibre systems in quasi-static three-point bending peak load confirms the positive hybrid effect, whose mechanism is now well-understood in terms of statistical fibre failure strain enhancement: carbon fibres adjacent to glass layers experience a localised strain redistribution that delays the catastrophic fibre fracture cascade. The 58 kN hybrid peak load versus 52 kN CFRP represents a 12% increase in specific bending resistance, consistent with the theoretical upper bound for 50% carbon volume fraction hybrids derived from classical laminate theory with progressive failure.

The three-stage stiffness degradation observed in CFRP is consistent with the progressive damage mechanics framework established by Reifsnider and Stinchcomb (1986), in which Stage I is dominated by transverse ply matrix microcracking (saturating at crack density approximately equal to 1–2 cracks/mm), Stage II by stable delamination growth at ply interfaces, and Stage III by fibre fracture cascade leading to final failure. The extended Stage II in CFRP — spanning approximately 70% of total fatigue life — has significant implications for structural health monitoring: acoustic emission sensors tuned to the 80–200 kHz frequency band associated with matrix cracking can detect Stage I onset with high reliability, providing approximately 70% of fatigue life as a monitoring window for scheduled maintenance.

The void–cure temperature relationship confirms the 60 °C cure onset as optimal for all three composite systems using LY1564 matrix. Void content above 2% has been shown by Bowles and Frimpong (1992) to reduce ILSS by approximately 7% per 1% void content increment — a relationship confirmed in the current dataset by the correlation between GFRP's higher void content (3.1%) and its lower ILSS relative to CFRP. This relationship underscores the manufacturing sensitivity of composite structural performance and the importance of process monitoring for critical structural components.

5. Conclusion

This multi-material fatigue study establishes that CFRP delivers the highest constant-amplitude fatigue life at all stress levels and the clearest three-stage stiffness degradation signature amenable to structural health monitoring, but at the highest CO_2 intensity (34.1 kg CO_2/kg) and material cost. The hybrid carbon–glass composite achieves the highest bending peak load due to the positive hybrid effect, offers superior post-peak ductility, and reduces CO_2 by 31% relative to CFRP with only 14% reduction in specific strength. GFRP provides the most favourable cost and environmental position but shows matrix-dominated, more variable fatigue failure. Cure temperature optimisation at 60 °C minimises void content in all systems; void fraction above 2% measurably reduces ILSS. TGA confirms all systems are thermally stable below 250 °C with glass transition temperatures between 121–138 °C. Hybrid composites are recommended for structural applications requiring the best balance of specific strength, fatigue resistance, bending ductility, and lifecycle CO_2 constraint.

References

[1] Bowles, K. J., & Frimpong, S. (1992). Void effects on the interlaminar shear strength of unidirectional graphite fibre reinforced composites. Journal of Composite Materials, 26(10), 1487–1509.

[2] Dijk, N. H. van, & Wagnac, E. (2021). Composite fatigue under variable amplitude loading. International Journal of Fatigue, 143, 106028.

[3] Hayashi, T. (1972). On the improvement of mechanical properties of composites by hybrid composition. Proceedings of the 8th International Reinforced Plastics Conference, London.

[4] Jeong, H. (2010). Effects of voids on the mechanical strength and ultrasonic attenuation of laminated composites. Journal of Composite Materials, 31(3), 276–292.

[5] Jones, R. M. (1999). Mechanics of Composite Materials (2nd ed.). Taylor & Francis, Philadelphia.

[6] Kawai, M., & Kato, K. (2006). Effects of R-ratio on the off-axis fatigue behaviour of CFRP composite at room temperature. International Journal of Fatigue, 28(10), 1277–1289.

[7] Mandell, J. F., & Samborsky, D. D. (1997). DOE/MSU Composite Material Fatigue Database (AANL Report SAND97-3002). Sandia National Laboratories.

[8] Nettles, A. T. (1994). Basic mechanics of laminated composite plates. NASA Reference Publication 1351, Marshall Space Flight Center.

[9] Reifsnider, K. L., & Stinchcomb, W. W. (1986). A critical element model of the residual strength and life of fatigue-loaded composite coupons. Composite Materials: Fatigue and Fracture, ASTM STP 907, 298–313.

[10] Sela, N., & Ishai, O. (1989). Interlaminar fracture toughness and toughening of laminated composite materials. Composites, 20(5), 423–435.

[11] Talreja, R. (1987). Fatigue of Composite Materials. Technomic Publishing, Lancaster.

[12] Toray Composite Materials America. (2018). T700S Data Sheet. CFA-007.

[13] Vassilopoulos, A. P. (Ed.). (2010). Fatigue Life Prediction of Composites and Composite Structures. Woodhead Publishing, Cambridge.